Full paper

A flexible hybridized electromagnetic-triboelectric multi-purpose self-powered sensor

Hassan Askari[a],[*], Zia Saadatnia[b], Ehsan Asadi[a], Amir Khajepour[a], Mir Behrad Khamesee[a], Jean Zu[b]

[a] Department of Mechanical and Mechatronics Engineering, University of Waterloo, 200 University Ave. West, Waterloo, ON, Canada N2L 3G1
[b] Department of Mechanical and Industrial Engineering, University of Toronto, Toronto, ON, Canada M5S 3G8

ARTICLE INFO

ABSTRACT

This paper presents a novel hybridized flexible electromagnetic-triboelectric generator that consists of a round/square shaped coil and magnet, and also, highly flexible, mechanically and thermally durable, and cost-effective polymeric materials. The reported hybridized nano generator is capable of converting external mechanical load to electricity. Using a systematic optimization approach results in an optimal configuration and size for the electromagnetic components of the self-powered sensor. Combination of the electromagnetic and triboelectric components provides several advantages for the proposed self-powered device including high resolution and power density even in low frequency and small amplitude of the excitations. We probe the sensitivity of the fabricated self-powered sensor considering different amplitude and frequency of excitations as well as external resistors. After providing a general performance analysis for the proposed self powered sensor, we show its potential for different specific applications including human motion based energy harvesting and sensing, tire condition monitoring, and pressure sensing. The utilization of the proposed self-powered sensor can provide a sustainable energy source for wireless sensor nodes, and also overcomes the battery capacity limitation that restricts the life time durability of mobile electrical devices.

1. Introduction

The efficient powering of wireless and embedded systems is still a major problem due to the dependence of such systems to batteries. For the systems with long operation time, energy is considered as a severe impasse, and accordingly, a number of researches have been accomplished so far to provide durable sources of energy for wireless and embedded systems. It is apparent that the lifetime of many sensor networks depends on service life of their energy sources, and thus, it is inescapable to implement new techniques for energy supplying to those systems.

Utilizing the accessible ambient sources of energy results in self-powered devices, which can be used in a large variety of applications including harsh and inaccessible environment of tires and turbines, monitoring crack formation in aircraft wings, on-line tracking of engine, detecting harmful chemical agents, monitoring tire conditions and human body motions. Self-powered sensor networks play a crucial role in promoting of our everyday life, and in fact, they are key technological instruments for industries with critical applications in environmental and infrastructure monitoring, health care, and most importantly, safety and security. During the last 2 decades, tremendous development of portable and personal electronic devices and their dependency to the power sources triggered researchers to implement and propose new techniques for self-powered sensing. Accordingly, four mechanisms have been proposed or used by researchers in self-powered instruments. These mechanisms include electrostatic, electromagnetic, piezoelectric and triboelectric approaches. This paper aims to propose a hybridized self-powered sensor with the fusion of electromagnetism and triboelectricity.

A few years after Faraday's scientific breakthrough in electromagnetic induction, electromagnetism fascinated researchers to implement it for electricity generation. Electromagnetic harvesters are basically developed in accordance with Faraday's law of electromagnetic induction. As a result, the electromagnetic harvester must be a combination of a coil and a magnet with a relative motion between them to produce energy. Indeed, the relative motion between a coil and a magnetic field causes a current to flow in the coil. Owing to low-cost and feasibility of the electromagnetic mechanism, it has been

Table 1
Recent Progress in Triboelectric Nano Generators.

Applications	Capability
Water wave energy harvesting	
-Broad frequency band blue energy harvesting [2]	-Maximum output power of 15.67 $\mu\frac{W}{cm^2}$
- Network of TENGs [3]	- Average output power of 1.15 $\frac{MW}{km^2}$
- Duck shaped TENG [4]	- Delivering power density of 1.366 $\frac{W}{m^2}$
- Spring assisted TENGs [5]	- Output power density of 726.48 $\frac{mW}{m^3}$.
Human motion based energy harvesting and sensing	
-Ultrathin flexible single-electrode TENGs [6]	-Instantaneous force sensing is about 0.947 μA Mpa^{-1}
-Skin inspired mechanically durable TENG [7]	-Maximum output power density of 0.5 $\frac{W}{m^2}$
-Powering wearable electronics by bio-mechanical energy [8]	-Capability of high surface density of 250 μCm^{-2}
-Random bio-mechanical energy for powering of mobile devices [9]	-Continuous power generating in the amount of (7.34 W m^{-3})
Tire and traffic condition monitoring	
-Scavenging friction energy from rolling tires [10]	- Achieving power of 1.79 mW at load resistance of 10 $M\Omega$
-Harvesting vertical rotation energy in broad frequency band [11]	- Maximum output power about 11 μW
-Rotating-disk-based for powering traffic volume sensor [12]	- Delivering output power of 17.5 mW and volume power density 55.7 $\frac{W}{m^3}$
Mass sensing	
- Molecular mass spectrometry [13]	- Highly sensitive mass sensing with resolution of 0.6 zeptomole
- Self-powered weighing [14]	- Capability of mass sensing and power generating about 10.3 μW
Pressure and Touch sensing	
- Real time tactile mapping [15]	- Visualization of touch actions or tracking motion trajectories in real-time.
- Flexible self-charging power film [16]	- Sliding unlock system in Touchpad Technology
- Flexible keyboard cover [17]	- 0.8 mJ electricity for 1 h typing

considered as a viable platform for a plenty of self-powered devices and also a reliable technique for energy harvesting. It has been implemented for energy harvesting from ocean, human walking, vehicle suspension, and wind. Implementing the electromagnetic energy harvester provides many advantages such as improving reliability and reducing the mechanical friction. In addition, there is no need for initial voltage source as the electrostatic mechanism requires [1].

Triboelectric nano generator (TENG),which operates based on the contact electrification effect and the electrostatic induction was firstly invented by Z.L. Wang in 2012. TENG has the capability of generating high open-circuit voltage even in oscillatory systems with low frequency and small amplitude. This unrivaled feature of the TENG have prompted researchers to implement them for plenty of applications including bio-instruments to ocean wave energy harvesting. Table 1 provides a summary of recently published papers based on TENG. As Table 1 shows, TENG has a significant potential for a plenty of applications in energy harvesting and self-powered sensing.

In order to benefit from the advantages of both EMG and TENG in a singular package, many devices have been invented so far using the hybridization technique. These novel devices have shown promising potential in self-powered watches, ocean wave energy harvesting, tire condition monitoring, traffic monitoring, safety helmet, and harsh environment. Table 2 provides a compendium of recently developed hybridized EMG-TENG self powered sensors and energy harvesters. As

Table 2 indicates, the developed hybridized self-powered systems can be used in thermal sensors, vibration monitoring instruments, acceleration sensor systems, detection of breath personality, and opto-electronics.

This research reports a multi-purpose self-powered device with many potential applications. The proposed self-powered sensor operates based on both electromagnetism and triboelectricty. In the first section of this work, we design the configuration of the system and optimize the electromagnetic parts. We consider both round and square configurations for the utilized magnet and coil in our flexible self-powered sensor. Combination of the electromagnetism and triboelectricity proposes many advantages in terms of both sensing and energy harvesting. The triboelectric part of the self-powered device consists of highly flexible, mechanically and thermally durable, and cost-effective polymeric materials. The contact-separation mode is taken into account for the design of the single electrode TENG part. A detailed analysis related to the application of single electrode triboelectric nanogenerator as a self-powered system can be found in Ref. [39].

In order to show the capability of the proposed self powered sensor, we perform a systematic experimental analysis with taking into account both energy harvesting and self-powered sensing features. The influence of the external circuit, triggering frequency and the amplitude of the oscillations are fully investigated. Experimental investigation results in finding the optimum external load for reaching the highest power density.

The last section of the paper represents the capability of the proposed self-powered sensor for three different applications. An interesting point about this sensor is its potential for multi-purpose applications. Although it has a simple structure, but it has the potential to be used in different engineering applications. Our first targeted application considers human-walking for both energy harvesting and sensing. Human walking is a rich source in terms of energy and also health condition monitoring. We also examine the potential of the proposed self-powered sensor for tire condition monitoring as another important application. The device shows auspicious potential for tire condition monitoring. The last case shows the stunning potential of the proposed device for the pressure sensing.

2. Design

This section fully describes design and working mechanism of the proposed self-powered harvester. We firstly introduce the electromagnetic component of the proposed system. In addition, a detailed geometry information is provided for EMG component,and also, we discuss its working mechanism. Section 3.1 describes design and working mechanism of TENG component of the proposed energy harvester. Fig. 1(a)-(b) schematically represents the proposed self-powered sensor with round PMs and coils and also its cross section view, respectively. Similarly, Fig. 1(c)-(d) schematically shows the system with square shape PMs and coils and also its cross section view, respectively. Fig. 1(e)-(f) shows the fabricated self-powered sensor with round and square shape PM and coils, respectively. The main structure of the self-powered sensor consists of two rectangular pieces of Viton rubber with length of 4.5 cm and width of 1 cm. These two Viton rubbers are attached by two glass pieces with thickness of 2.5 mm, height of 9 mm, and width of 1 cm.

2.1. EMG structure and working mechanism

As indicated in Fig. 1, we designed two types of hybridized sensors with similar configuration. The first one contains a cylindrical permanent magnet (gray color), and a cylindrical coil (copper color). The second design includes a square shape permanent magnet and coil. Each coil has an iron core as indicated in the Figure. The permanent magnet is located on top of the rubber and the coil is placed under the Kapton as indicated in Fig. 1. The iron core closes the magnetic flux

Table 2

Hybridized triboelectric-electromagnetic self-powered sensor and energy harvester.

Device	Applications
-Electromagnetic-triboelectric-thermoelectric nano generator [18]	-Scavenging bio-mechanical energy for lighting up globe lights and charging cell-phone.
- Self-powered safety helmet [19]	- Lighting up 1000 LEDs for emergency application
-Rotating-disk-based-hybridized EMG-TENG [20,21]	-Powering wireless traffic volume sensors and a mobile electrical devices
- Hybridized rolling EMG-TENG nano generator [22]	-Harvesting water motion energy
-A water proof hybridized EMG-TENG [23]	-Harvesting wind energy in the rainy condition and water-flow energy under water
-Self-powered electronic watch [24]	-Powering self-powered watch
-Air-flow energy harvester [25,26]	-Sustainably powering temperature sensors
-Bio-mechanical energy scavenger [27]	-Sustainably powering wearable electronics and wind energy harvesting
-Magnetically levitated TENG-EMG [28]	- Self-powered vibration monitoring sensor
-Traffic monitoring hybridized EMG-TENG [29]	-Energy harvesting and traffic monitoring
-Ferrofluid-based hybridized EMG-TENG [30]	-For sensitive and sustainable vibration energy harvesting
-Noncontact EMG-TENG hybrid nanogenerator [31]	-Scavenging biomechanical energy
Conductive Fabric-Based Stretchable nanogenerator [32]	-Scavenging biomechanical Energy
-Shared-electrode-based hybridized EMG-TENG [33]	-Self powered acceleration sensor systems
-Magnetic-assisted noncontact TENG [34,35]	-Magnetic sensor, self-powered electronics, optoelectronics, water and wind based energy harvesting
-Linear grating hybridized TENG-EMG [36]	-Sustainably powering portable electronics
-Magnetic-assisted triboelectric nanogenerators [35]	-Self-powered visualized omnidirectional tilt sensing system
-Broadband nonlinear hybridized TENG-EMG energy harvester [37]	- Self-powered acceleration sensor
-Foldable and portable hybridized TENG-EMG [38]	-Sensitive gas flow sensor for detecting breath personality

circuits, and thus, enhances the energy regeneration rate. Table 3 provides the details relevant to the geometry and properties of both coils and magnets. The electromagnetic component of the hybrid design functions based on the Faraday and Len'z laws. Faraday's law of induction states that the change of the total flux in a closed circuit results in an induced electromotive force proportional to the rate of change of flux through the integral path. According to the Lenz's Law, the induced magnetic field produced by the induced current will oppose the direction of the original magnetic field. Applying an external force,pressure or moment on the fabricated sensor causes a relative displacement between the magnet and the coil, resulting in currents inside the coil wire turns, and thus, generating voltage.

2.2. TENG structure and working mechanism

TENG component of the self-powered sensor contains a layer of Polyurethane and a layer of Kapton with a thin Aluminum electrode on its bottom. As represented in Fig. 1, Kapton layer is located on the top

Table 3

Geometry of the magnets,coils and iron cores.

Components	Thickness	Size	Turns	B_r	AWG
Round Coil	4 mm	R = 1 cm	73	○	30
Square Coil	4 mm	L = 1 cm	73	○	30
Round PM	1/8 in	R = 3/8 in	○	1.35 T	○
Square PM	1/8 in	L = 3/8 in	○	1.35 T	○
Round core	4 mm	R = 6.35 mm	○	○	○
Square core	4 mm	L = 6.35 mm	○	○	○

surface of the coil. The location of Polyurethane is under the PM. The working mechanism of the TENG component is schematically depicted in Fig. 2 which is based on the conjunction of contact electrification and electrostatic induction [1]. When the device is being pressed, the surfaces of Kapton and Polyurethane are fully in contact so that the charges will be transferred between them, as shown in Fig. 2(a). The reason is that the Kapton layer is more triboelectrically negative than
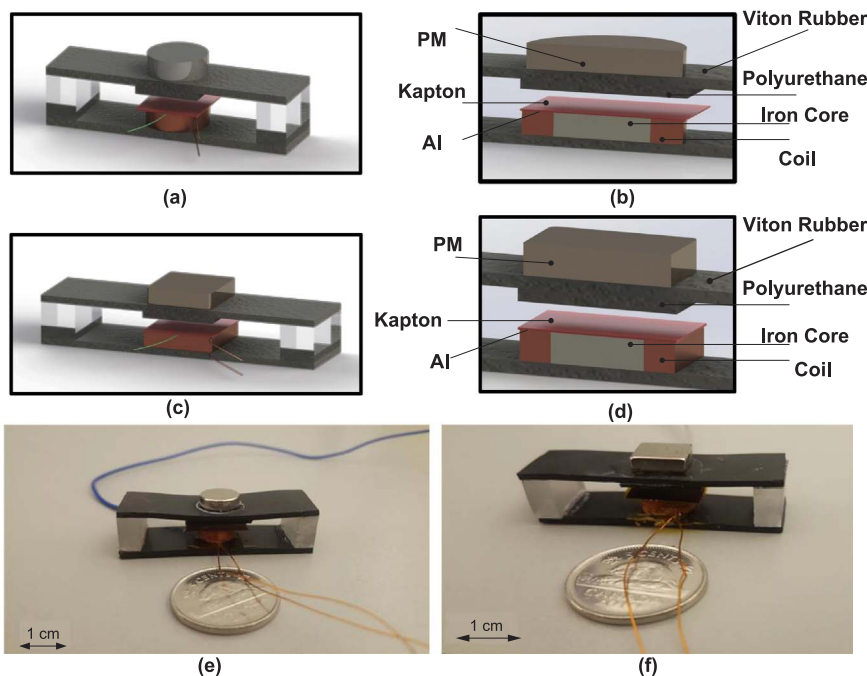

Fig. 1. Schematic of the proposed hybrid electromagnetic-triboelectric generator: (a) circular shape PM and coil (b)Cross section view of circular shape, (c) square shape PM and coil, (d)Cross section view of square shape; As-fabricated hybrid electromagnetic-triboelectric generator: (e) circular shape PM and coil (f) square shape PM and coil.
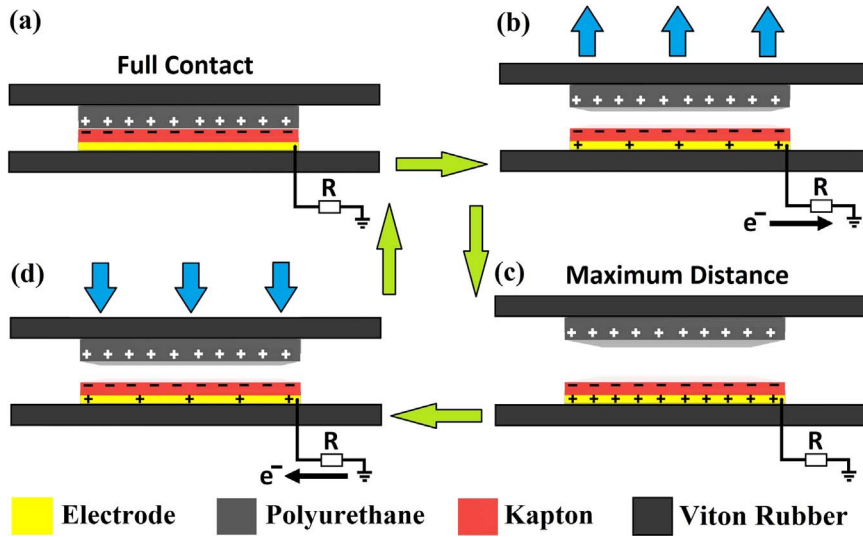
(a)

Full Contact

(b)

(d)

(c) **Maximum Distance**

■ **Electrode**   ■ **Polyurethane**   ■ **Kapton**   ■ **Viton Rubber**

Fig. 2. Mechanism of the TENG component of the self-powered sensor under one cycle of pressing and releasing.

Polyurethane and therefore electrons are transferred to the Kapton surface. The Kapton layer holds negative charges while the Polyurethane surface obtains similar magnitude of charges with opposite polarities to maintain the charge balance. In this condition, there is no electron flow between the electrode and the ground, which are connected to each other through an external electrical load. As the Polyurethane layer departs the bottom layer, the local electrical field distribution will be changed leading to the electron flow from the electrode toward the ground, as seen in Fig. 2(b). The maximum charge transfer is obtained when the top layers reaches to a specific distance where the charge balance is fully achieved, as depicted in Fig. 2(c). Similarly as the Polyurethane approaches the bottom layer, the electrons are driven back through the external load to maintain the balance until reaching the full contact (Fig. 2 (d)). Therefore, such process will result in an electricity generation through the load with an alternative manner.

3. Mathematical model

3.1. Electromagnetic model

The dominant principle in electromagnetic modelling is Faraday and Lenz's laws of induction. In accordance with these combined laws, we have the following general formulation for the electro-motive force (emf) across the coils:

$$V_{emf} = -\int_C (E + v \times B) \cdot dl \tag{1}$$

where V_{emf} represents the emf in volts, E and B are electric and magnetic fields, dl is an infinitesimal vector element of the coils wire with a velocity of v. After finding the V_{emf}, using the Faraday-Lenz's law, the induced current (i) and regenerated power (P_e) of the coil are determined using the following relations:

$$L_{coil}\frac{di}{dt} + (R_{coil} + R_{ext})i = V_{emf} \tag{2}$$

$$P_e = R_{ext} i^2 \tag{3}$$

where L_{coil} and R_{coil} are inductance and resistance of the coil respectively, and R_{ext} is the resistance of external load connected to the coil. Finding an accurate closed form magnetic field for the considered configuration (coil with iron core) is significantly complicated. However for the case of having no iron core in both round and square cases, we can obtain a closed form for the components of the magnetic field in coil wires. For a cylindrical permanent magnet of radius R_{pm} and length h_{pm}, and remnant magnetic flux density of B_r the produced

magnetic field at any location (r,z) is given by [40]:

$$B_r = B_0[\alpha_+ C(k_+, 1, 1, -1,) - \alpha_+ C(k_-, 1, 1, -1,)] \tag{4}$$

with

$$B_0 = \frac{B_{rem}}{\pi} \tag{5}$$

The coefficients of Eq. (4) are defined as below based on Ref. [40]:

$$z_\pm = z \pm \frac{h_{pm}}{2} \tag{6}$$

$$\alpha_\pm = \frac{R_{pm}}{\sqrt{z_\pm^2 + (r + R_{pm})^2}} \tag{7}$$

$$\beta_\pm = \frac{z_\pm}{\sqrt{z_\pm^2 + (r + R_{pm})^2}} \tag{8}$$

$$\gamma = \frac{R_{pm} - r}{R_{pm} + r} \tag{9}$$

$$k_\pm = \frac{\sqrt{z_\pm^2 + (R_{pm} - r)^2}}{\sqrt{z_\pm^2 + (R_{pm} + r)^2}} \tag{10}$$

where C represent a generalized complete elliptic integral given by:

$$C(k_c, p, c, s) = \int_0^{\pi/2} \frac{c\cos^2\phi + s\sin^2\phi}{(\cos^2\phi + p\sin^2\phi)\sqrt{\cos^2\phi + k_c^2\sin^2\phi}}d\phi \tag{11}$$

A detailed analysis for the magnetic field of square shape magnet can be found in ref. [41]

4. Results and discussion

4.1. Finite element analysis

This section provides the finite element analysis for both EMG and TENG components. Fig. 3(a)–(d) shows the radial magnetic flux density at different locations obtained by COMSOL® multiphysics software package (version:5.2a) for EMG component with round coil and PM. Fig. 3(a) represents a 2D view of the radial magnetic flux density of the EMG component with iron core. Fig. 3(b) shows a 3D view of magnetic flux density of the EMG component with iron core. Fig. 3(c)-(d) illustrate 2D and 3D views of the magnetic flux density of the EMG components without iron core. It must be highlighted that using iron core increases the maximum of the radial magnetic flux density in coil from 0.11758 *T* to 0.30304 *T*. It is a significant increase as we expected based
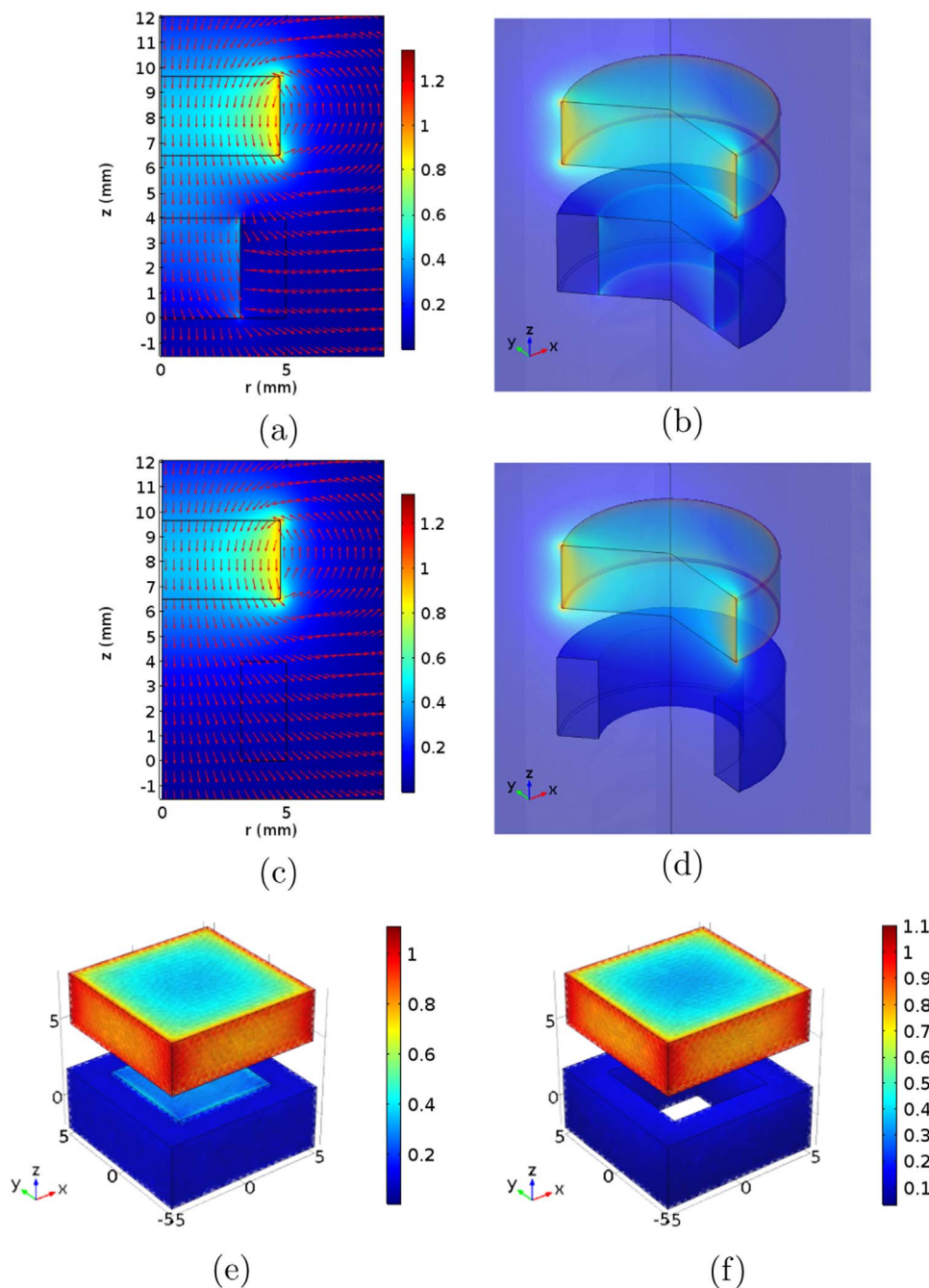
on our optimization results, which is presented in Section 4.2. Fig. 3(e) and (f) represent the magnetic flux density in square shape coil and magnet with and without iron core, respectively. Similar to the round shape, the magnetic flux density increases with implementing the iron core.

In order to analyze the operation of the TENG component, we carried out a finite element model in COMSOL® software, as schematically shown in Fig. 4(a). We calculated the electric potential distribution in the open circuit (OC) condition by changing the distance between the top and bottom layers. The Kapton layer and attached electrode was fixed, and the external excitation results in changing the position of Polyurethane layer. The 2D model was taken into the account due to the very small thickness of contact layers in comparison with other dimensions of the layers. The surface charge density of 25 NC/m^2 was typically assigned to the top surface. Also, we assigned a similar magnitude of the surface charge density but with an opposite polarity to the

bottom surface. The charges were uniformly distributed on the contact surfaces owing to the insulation properties of the selected materials [2]. The potential at infinity was taken as the reference condition and the entire system was surrounded by air same as the real experimental condition [1]. Figs. 4(b)–(d) show variation of the potential distribution when the distance changes from zero to the maximum condition. Accordingly, the electric potential is increased as the top layer departs from the bottom layer. Fig. 4(e) shows the variation of open-circuit voltage V_{oc} with respect to the relative displacement (y/y_{max}). The voltage is increased by raising the top layer indicating the generation of electricity when the system is being pressed and released.

4.2. EMG optimization

In order to maximize the performance of the system in terms of power harvesting, an optimization is performed to select the
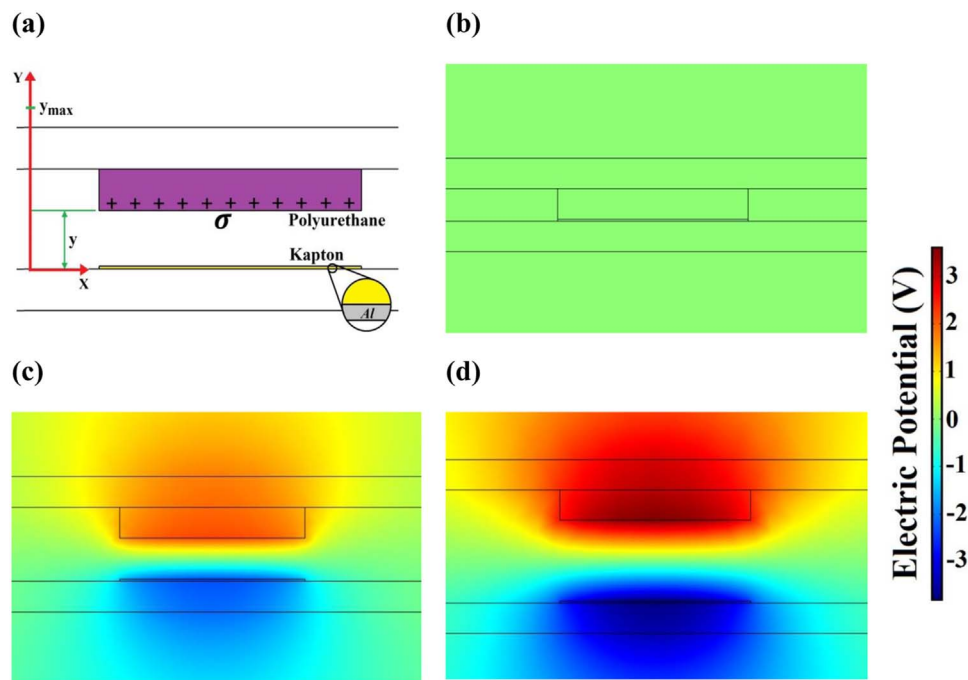
Fig. 4. (a) FEA model for the TENG component. (b)-(d) Electric potential distribution for $\frac{y}{y_{max}} = 0$, 0.5, 1. (f) Open-circuit voltage with respect to the relative displacement.
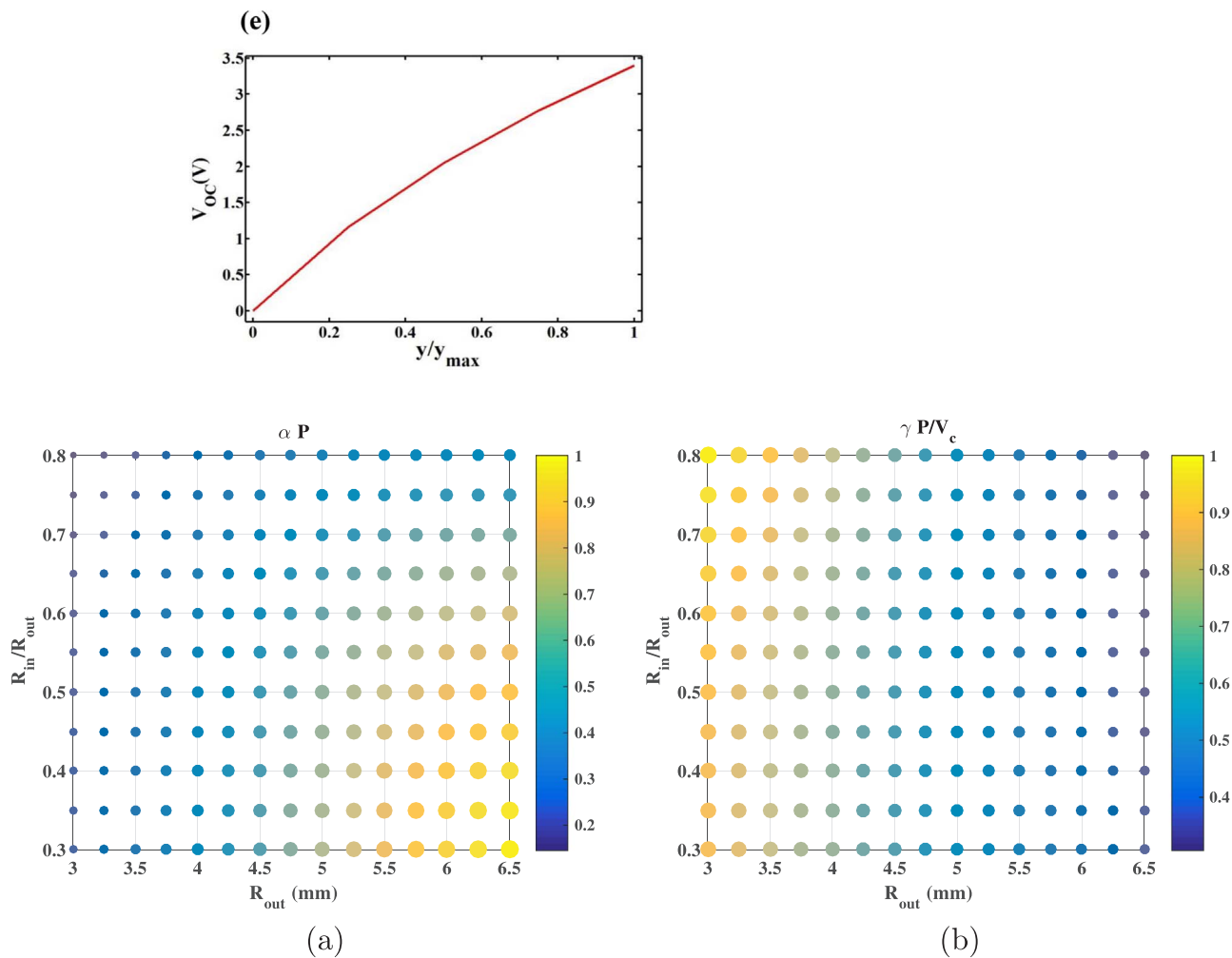

Fig. 5. Optimization Results (a) Variation of output power with respect to the ratio of inner diameter to outer diameter, and also outer diameter, (b) Power density (power to coil volume).
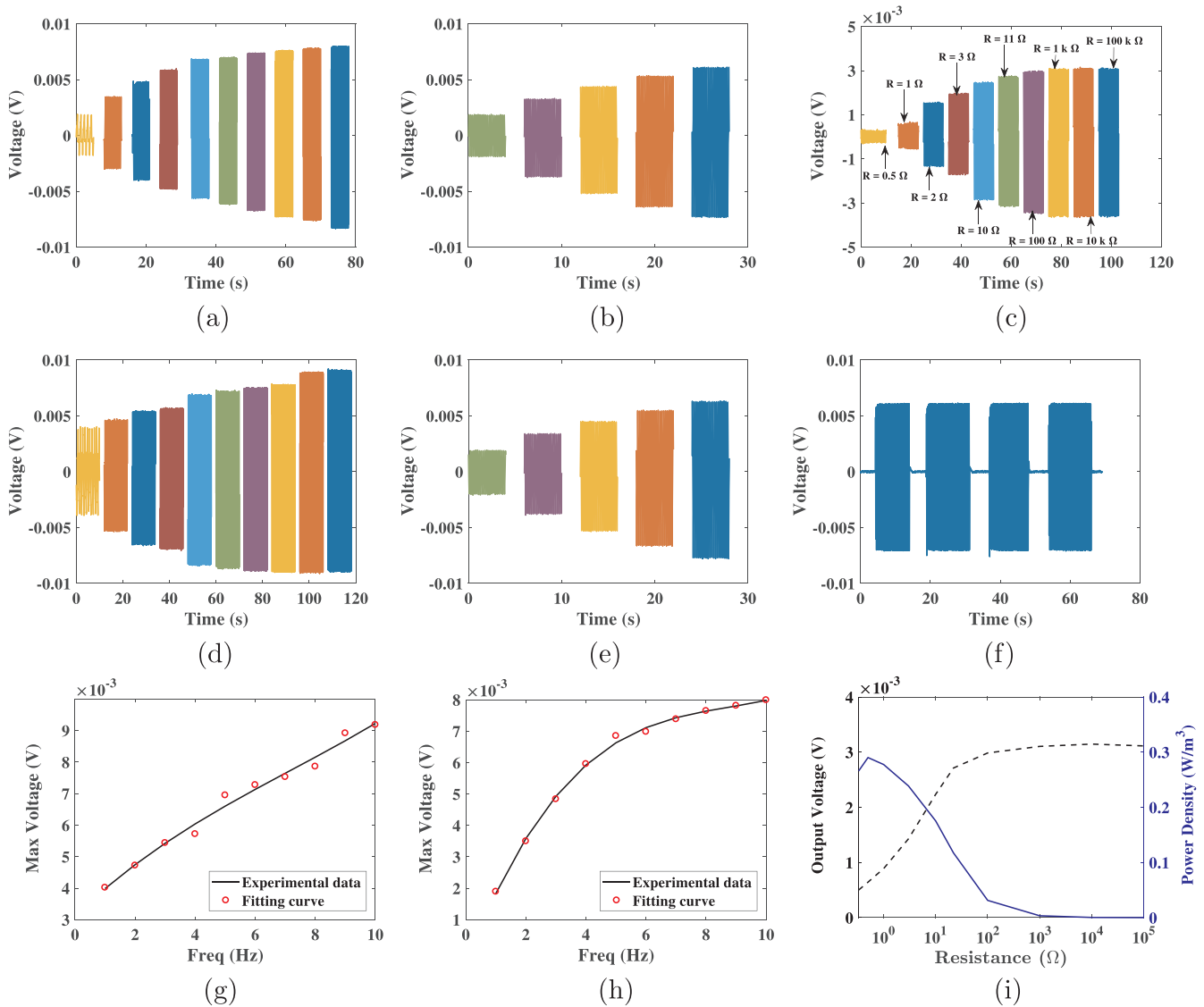
Fig. 6. Electrical output of the sensor; round PM and coil: (a) Effect of frequency on open circuit voltage, (b) Effect of amplitude of excitation on open circuit voltage, (c) Effect of external resistance on open circuit voltage; square PM and coil: (d) Effect of frequency on open circuit voltage, (e) Effect of amplitude of excitation on open circuit voltage, (f) Durability test(Turn on-off); effect of frequency on maximum voltage of the EMG component:(g) with square PM and coil, (h) with round PM and coil, (i) power density and output voltage versus external resistance.

dimensions of the electromagnetic component. The magnet should be selected based on the availability in the market. Furthermore, the allocated space for the magnet and coil is limited. Considering these two constraints, a magnet with diameter of 3/8 *in* and thickness of 1/8 *in* is selected from the market. For the coil dimensions, a thickness of 4 mm is chosen to fit inside the sensor. The remained parameters for optimization are the inner and outer radius of electromagnetic coil. Fig. 5 (a) and (b) represent the harvested power and power densities (power to coil volume ratio) of the electromagnetic component respectively, for different coil outer radius and different coil outer to inner radius rations. It should be noted that, the obtained valued are multiplied by two constants (α and γ for Fig. 5 (a) and 5 (b) to normalize the results). As it can be seen, generally by increasing the size of the coil, the harvested power increases (i.e larger R_{out} and smaller R_{in}/R_{out}), however, the best power density is obtained for a smaller coil (i.e. smaller R_{in} and larger R_{in}/R_{out}). Thus, there is trade off between higher power and higher power density. For this work, we selected the values of 5 and 0.635 for R_{out} and R_{in}/R_{out} respectively, to obtain a good compromise of power and power densities.

4.3. Sensor performance

For the purpose of analyzing the performance of the hybrid self-powered sensor, we investigate the effect of the external resistive load,amplitude of the deflection, frequency of the excitation for all of the components of the self-powered sensor. The performance of the sensor has been studied in both general and special cases. The special cases include human walking, tire condition monitoring as well as pressure sensing. In order to characterize the capability of the sensor, the electrical output of the sensor is experimentally obtained. In each set of experiments, EMG and TENG components, which is being tested, are shunted with a variable external resistance. All of the voltage data are collected via MATLAB windows real time target toolbox using an NI-6221 DAQ. The displacement is measured using a Celessco SP2 string potentiometer. A LDS 721 shaker is employed to excite the sensor at different frequencies and amplitudes. The shaker is adjusted to apply sinusoidal displacement using a 33220 A Agilent function generator. Fig. 6 shows the electrical output of the EMG component of the self-powered sensor. Fig. 6(a) represents the effect of frequency on the open circuit voltage of the EMG component. As indicted, increasing of the
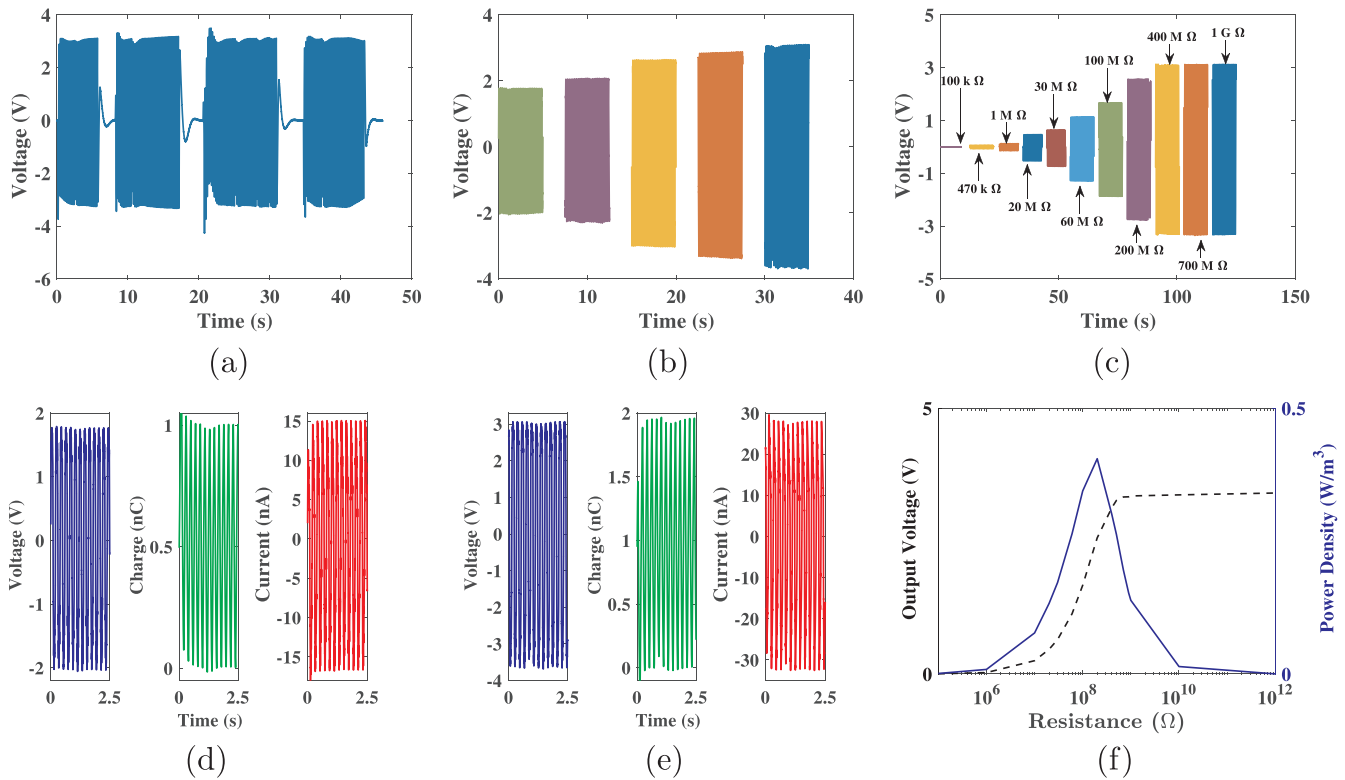
Fig. 7. Electrical output of the sensor -TENG component (a) Durability test(Turn on-off) (b) Effect of amplitude of excitation open circuit voltage, (c) Effect of external resistance on open circuit voltage, (d-e) open circuit voltage, transferred charge, and short circuit current-TENG component for the smallest and the highest amplitudes of excitation, respectively, (f)Power density and open circuit voltage versus external resistive load.

frequency results in enhancing its open circuit voltage. Fig. 6(b) represents the effect of amplitude of excitation. As the shaker amplitude of excitation increases, the voltage of the EMG component increases. Fig. 6(c) depicts the effect of external resistance on the performance of the EMG components. As expected, increasing the external resistance results in increasing of the EMG component voltage. A similar study is performed on the proposed self-powered sensor with square shape coil and PM. Fig. 6 (d) shows the influence of excitation frequency on the open circuit voltage of the sensor with square shape coil and PM. As the frequency of excitation increases, its corresponding voltage enhances. This is what we expect from the EMG component. Fig. 6(e) represents the effect of excitation amplitude on the voltage of the system. As shown in Fig. 6(e), the open circuit voltage increases with increasing of the excitation amplitude. We turned off the shaker and turned it on again to evaluate the performance for this case, as indicated in Fig. 6(f). What stands out in the Fig. 6(f) is the durability of the EMG component. As presented, the sensor voltage comes back to its original performance after its being turned on again. Fig. 6(g) represents the effect of frequency on the maximum open circuit voltage for square shape coil and PM. As indicated in figure, by increasing the frequency from 1 Hz to 9 Hz, the open circuit voltage increases from 4 mV to 9.1 mV. Similar study is performed for the sensor with round shape coil and PM as represented in Fig. 6(h). From the figures, it can be seen that the sensor with square shape has a higher electrical output comparing with the round shape. Fig. 6(i) illustrates the variation of the power density for the EMG component. As depicted by Fig. 6(i), the power density increases with increasing the external shunted resistance and reaches its zenith when the external shunted resistance equals to the coil resistance. Fig. 7 shows the performance of TENG component of the sensor. In order to see the durability of the TENG component, we turned off the shaker and turned it on again to evaluate the sensor durability performance, as indicated in Fig. 7(a). Fig. 7(b) shows the effect of the amplitude of the shaker's excitation on the open circuit voltage of the

sensor. As the shaker's excitation increases, the amplitude of open circuit voltage increases for the TENG component. Fig. 7(c) represents the influence of the external shunted resistance on the performance of the TENG component. As depicted by Fig. 7(c), increasing the resistance results in enhancing the open circuit voltage of the TENG component. Fig. 7(d)-(e) show the open circuit voltage, short circuit current and transferred charge of TENG component. Comparing these three figures illustrates the effect of amplitude of oscillations on TENG performance. As depicted by figures, increasing the amplitude of oscillations enhances the open circuit voltage, short circuit current and transferred charge. Fig. 7(f) illustrates the variation of the power density for the TENG component. By increasing the external resistance, both output voltage and power density of the TENG component increase. Power density starts decreasing right after its maximum point at the optimal shunted resistance.

4.4. Special applications

In this section, we investigate the capability of as-fabricated self-powered system for three different applications. The self-powered sensor has been employed for three different cases including human walking, tire condition monitoring, and and also pressure sensing.

4.4.1. Case 1: Human walking

The first special case is based on human walking. We know that human walking contains lots of information about the body, and in fact, our motion monitoring can lead to providing useful information about our health. In addition, human walking is a rich source of kinetic energy. In order to evaluate the capability of our sensor for human-walking based energy harvesting and sensing, we attached it to a shoe as represented in Fig. 8(c). Then, we obtained the open circuit voltage for both EMG and TENG component for a regular walking speed. As can be seen by the Fig. 8(a), the EMG component of the attached sensor is
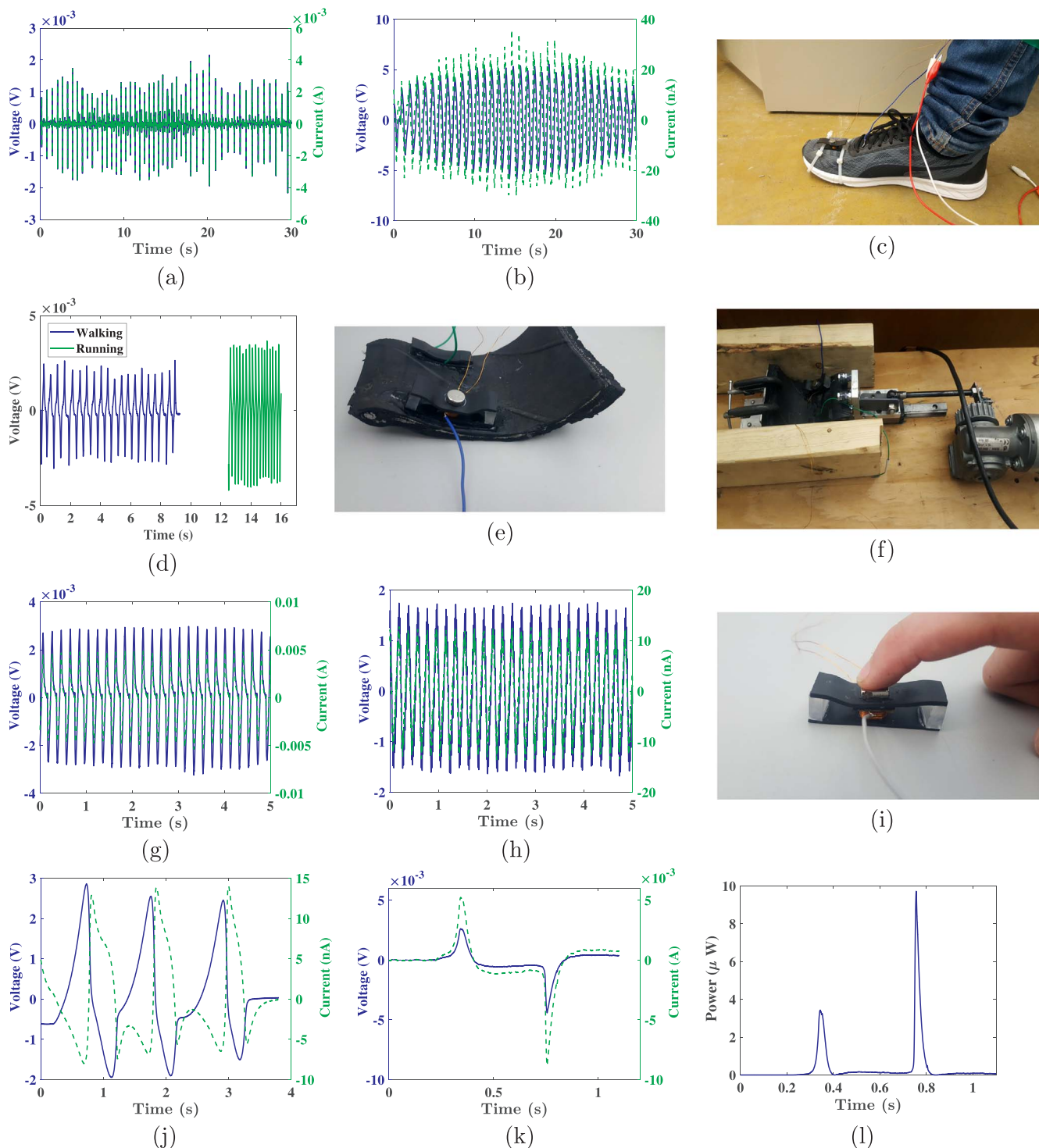
Fig. 8. **Case 1**: (a) Open circuit voltage and short circuit current of the EMG component based on human walking, (b) Open circuit voltage and short circuit current of the TENG component based on human walking (c) A shoe equipped by as-fabricated self-powered sensor (d) EMG component open voltage circuit in walking and running cases; **Case 2**: (e)Side-wall of the tire along with the attached sensor, (f) Experimental setup (g) Open circuit voltage and short circuit current of the EMG component (h) Open circuit voltage and short circuit current of the TENG component;**Case 3**: (i) The fabricated sensor under finger pressure, (j) Open circuit voltage and short circuit current of the sensor under different finger press-release loads- TENG component(k) Open circuit voltage and short circuit current of the sensor under a finger press-release load- EMG component, (l) Output power of the sensor under a finger press-release load- EMG component.

capable of generating about 4 mV peak-peak open circuit voltage at its maximum point. The maximum peak to peak short circuit current for the EMG component is around 8 mA. Similarly, TENG component represents promising results with approximately 10 peak-peak open circuit voltage at its maximum level. Fig. 8(d) represents the performance of the system in both walking and running speed.

4.4.2. Case 2: Tire condition monitoring

As the second special application, we probe the performance of the proposed system as a self-powered sensor for tire condition monitoring. Tire condition monitoring is a very important topic in the area of vehicle dynamics and it is still a challenging area of research due to the harsh environment of the tire, and also its stochastic dynamics. It is

vital to fabricate a sensor which is capable of measuring different forces, pressure, and moments in a tire. In this part, we show that the developed sensor has the capability of tire condition monitoring. We attached the sensor to the sidewall of the tire, as shown in Fig. 8(e), and then to trigger the attached sensor, we applied a periodic force with a crank-slider mechanism along with a rotating crank, a connecting rod and a reciprocating slide as represented in Fig. 8(f). Fig. 8(g) shows the open circuit voltage and short circuit current of the EMG component of the attached sensor. As indicated, a clear and illustrative signal is obtained based on the EMG component. The peak-peak open circuit voltage and short circuit current of the EMG component are about 5.2 mV and 10 mA, respectively. Fig. 8(h) shows the open circuit voltage and short circuit current obtained from the TENG component of the attached system. As illustrated in the figure, the peak-peak open circuit voltage and short circuit current for the TENG component is about 3.2 V and 25 nA. The results of these two figures represent a high potential of the fabricated sensor for tire condition monitoring. With a properly trained neural network, the measured signals can be translated to the dynamical parameters of the tire such as forces, moments and pressure.

4.4.3. Case 3: Pressure sensing

The last special case considers a very interesting application for the as-fabricated sensor. We studied the performance of the self-powered sensor for pressure sensing. Our experimental results show promising potential of the device for pressure sensing. We exerted different pressure loads on top of the sensor as shown in Fig. 8(i). Fig. 8(j) shows the open circuit voltage and short circuit current of the TENG component of the self-powered sensor under different finger pressure loads. As delineated in the figure, by decreasing the finger pressure, the open circuit voltage of the TENG component decreases. It must be noted that each pair of subsequent positive and negative peaks are related to each press and release of the finger pressure on top of the sensor. The first positive peak stands for the first pressure, which is the highest finger pressure that we applied for investigating the effect of pressure in our experiment. The first negative peak is related to releasing the finger pressure after applying the highest pressure to the sensor. In the second pair of the peak voltages, we reduced the amount of the finger pressure, therefore, as it can be seen from the figure, the peaks of the voltage for both press and release cases decrease. The last pair of peaks are related to the lowest amount of the finger pressure that we applied on top of the fabricated device. As expected, the lowest peaks are obtained for this case. Thus, we can conclude that with a higher finger pressure, the device will generate a higher electrical output. Our device shows comparably high sensitivity considering the results of other proposed nanogenerators for finger pressure sensing. As one of the examples of the nanogenerators, which has been tested under finger pressure, we can refer to a paper by Chen et al. [42]. They reported a piezoelectric nanogenerator, which is capable of generating the maximum voltage of 1.6 V. Also, their results show that their proposed device can generate about 0.4 V under finger pressure. In another example, Ahmed et al. designed a self-powered keyboard based on triboelectric nanogenerators, and showed that their fabricated device is capable of generating 1.5 V in water and 0.4 V in air under gentle finger pressure [43].

Fig. 8(k) represent the open circuit voltage and the short circuit current of the EMG component under a press-release force. Fig. 8(l) depicts the output power of the self-powered sensor EMG component. Based on the presented results in Fig. 8(j)–(l) and considering the high output power of the EMG component, this device shows a high potential for pressure sensing. Comparing with the previously published articles, the flexibility and also stiffness of the device comes from the structure of the system,and therefore, it does not require a spring to provide the stiffness. This helps to reduce the extra cost and also the weight of a spring [27]. Comparing with Refs. [36,44], the proposed device of the present research operates based on the contact-separation mode. In addition, it has more flexibility in comparison with the proposed self-powered device in Ref. [36].

5. Conclusion

A novel type of flexible self-powered sensor was presented with combination of EMG and TENG. The design of the structure of both EMG and TENG components was fully discussed. In addition, the working mechanism of the both components were fully discussed. An optimization analysis was utilized to design the EMG component of the proposed self-powered sensor. A finite element analysis was also performed to investigate the capability of the proposed system. A comprehensive experimental analysis was carried out to study as-fabricated self-powered sensor under different dynamical and electrical conditions. Results of the paper show that increasing the amplitude of oscillations results in increasing the open circuit voltage of both EMG and TENG components of the device. Similarly, increasing the external shunted resistance enhances output voltage of both EMG and TENG components of the fabricated sensor. The as-fabricated sensor was used for three different specific applications including human motion based energy harvesting and sensing,tire condition monitoring, and pressure sensing. The fabricated device represents promising potential for all of the above-mentioned targeted applications. The findings of this study suggest that the proposed flexible self-powered sensor can be exploited in several different applications, and it can be considered as a multi-purposed self-powered sensor.

References

[1] Ö. Zorlu, E.T. Topal, H. Kulah, A vibration-based electromagnetic energy harvester using mechanical frequency up-conversion method, IEEE Sens. J. 11 (2) (2011) 481–488.

[2] Z. Wen, H. Guo, Y. Zi, M.-H. Yeh, X. Wang, J. Deng, J. Wang, S. Li, C. Hu, L. Zhu, et al., Harvesting broad frequency band blue energy by a triboelectric-electromagnetic hybrid nanogenerator, ACS Nano 10 (7) (2016) 6526–6534.

[3] J. Chen, J. Yang, Z. Li, X. Fan, Y. Zi, Q. Jing, H. Guo, Z. Wen, K.C. Pradel, S. Niu, et al., Networks of triboelectric nanogenerators for harvesting water wave: a potential approach toward blue energy energy, ACS Nano 9 (3) (2015) 3324–3331.

[4] A. Ahmed, Z. Saadatnia, I. Hassan, Y. Zi, Y. Xi, X. He, J. Zu, Z.L. Wang, Self-powered wirelesssensor node enabled by a duck-shaped triboelectric nanogenerator for harvesting water wave energy, Adv. Energy Mater. (2017).

[5] T. Jiang, Y. Yao, L. Xu, L. Zhang, T. Xiao, Z.L. Wang, Spring-assisted triboelectric nanogenerator for efficiently harvesting water wave energy, Nano Energy 31 (2017) 560–567.

[6] S.W. Chen, X. Cao, N. Wang, L. Ma, H.R. Zhu, M. Willander, Y. Jie, Z.L. Wang, An ultrathin flexible single-electrode triboelectric-nanogenerator for mechanical energy harvesting and instantaneous force sensing, Adv. Energy Mater. 7 (1) (2017) (1601255–n/a).

[7] Y.-C. Lai, J. Deng, S. Niu, W. Peng, C. Wu, R. Liu, Z. Wen, Z.L. Wang, Electric eel-skin-inspired mechanically durable and super-stretchable nanogenerator for deformable power source and fully autonomous conformable electronic-skin applications, Adv. Mater. 28 (45) (2016) 10024–10032.

[8] J. Wang, S. Li, F. Yi, Y. Zi, J. Lin, X. Wang, Y. Xu, Z.L. Wang, Sustainably powering wearable electronics solely by biomechanical energy, Nat. Commun. 7 (2016).

[9] S. Niu, X. Wang, F. Yi, Y.S. Zhou, Z.L. Wang, A universal self-charging system driven by random biomechanical energy for sustainable operation of mobile electronics, Nat. Commun. 6 (2015).

[10] Y. Mao, D. Geng, E. Liang, X. Wang, Single-electrode triboelectric nanogenerator for scavenging friction energy from rolling tires, Nano Energy 15 (2015) 227–234.

[11] J. Chen, H. Guo, G. Liu, X. Wang, Y. Xi, M.S. Javed, C. Hu, A fully-packaged and robust hybridized generator for harvesting vertical rotation energy in broad frequency band and building up self-powered wireless systems, Nano Energy 33 (2017) 508–514.

[12] B. Zhang, J. Chen, L. Jin, W. Deng, L. Zhang, H. Zhang, M. Zhu, W. Yang, Z.L. Wang, Rotating-disk-based hybridized electromagnetictriboelectric nanogenerator for sustainably powering wireless traffic volume sensors, ACS Nano 10 (6) (2016) 6241–6247.

[13] A. Li, Y. Zi, H. Guo, Z.L. Wang, F.M. Fernández, Triboelectric nanogenerators for sensitive nanocoulombmolecular mass spectrometry, Nat. Nanotechnol. (2017).

[14] S.A. Khan, H.L. Zhang, Y. Xie, M. Gao, M.A. Shah, A. Qadir, Y. Lin, Flexible triboelectric nanogenerator based on carbon nanotubes for self-powered weighing, Adv. Eng. Mater. (2016).

[15] X. Wang, H. Zhang, L. Dong, X. Han, W. Du, J. Zhai, C. Pan, Z.L. Wang, Self-powered high-resolution and pressure-sensitive triboelectric sensor matrix for real-time tactile mapping, Adv. Mater. 28 (15) (2016) 2896–2903.

[16] J. Luo, W. Tang, F.R. Fan, C. Liu, Y. Pang, G. Cao, Z.L. Wang, Transparent and flexible self-charging power film and its application in a sliding unlock system in touchpad technology, ACS Nano 10 (8) (2016) 8078–8086.

[17] S. Li, W. Peng, J. Wang, L. Lin, Y. Zi, G. Zhang, Z.L. Wang, All-elastomer-based triboelectric nanogenerator as a keyboard cover to harvest typing energy, ACS Nano 10 (8) (2016) 7973–7981.

[18] X. Wang, Z.L. Wang, Y. Yang, Hybridized nanogenerator for simultaneously scavenging mechanical and thermal energies by electromagnetic-triboelectric-thermoelectric effects, Nano Energy 26 (2016) 164–171.

[19] L. Jin, J. Chen, B. Zhang, W. Deng, L. Zhang, H. Zhang, X. Huang, M. Zhu, W. Yang, Z.L. Wang, Self-powered safety helmet based on hybridized nanogenerator for emergency, ACS Nano 10 (8) (2016) 7874–7881.

[20] B. Zhang, J. Chen, L. Jin, W. Deng, L. Zhang, H. Zhang, M. Zhu, W. Yang, Z.L. Wang, Rotating disk based hybridized electromagnetic triboelectric nanogenerator for sustainably powering wireless traffic volume sensors, ACS Nano 10 (6) (2016) 6241–6247.

[21] X. Zhong, Y. Yang, X. Wang, Z.L. Wang, Rotating-disk-based hybridized electro-magnetic-triboelectric nanogenerator for scavenging biomechanical energy as a mobile power source, Nano Energy 13 (2015) 771–780.

[22] X. Wang, Z. Wen, H. Guo, C. Wu, X. He, L. Lin, X. Cao, Z.L. Wang, Fully packaged blue energy harvester by hybridizing a rolling triboelectric nanogenerator and an electromagnetic generator, ACS Nano 10 (12) (2016) 11369–11376.

[23] H. Guo, Z. Wen, Y. Zi, M.-H. Yeh, J. Wang, L. Zhu, C. Hu, Z.L. Wang, A water-proof triboelectric-electromagnetic hybrid generator for energy harvesting in harsh environments, Adv. Energy Mater. 6 (6) (2016) 1501593, http://dx.doi.org/10.1002/aenm.201501593 1501593–n/a.

[24] T. Quan, X. Wang, Z.L. Wang, Y. Yang, Hybridized electromagnetictriboelectric nanogenerator for a self-powered electronic watch, ACS Nano 9 (12) (2015) 12301–12310.

[25] X. Wang, S. Wang, Y. Yang, Z.L. Wang, Hybridized electromagnetictriboelectric nanogenerator for scavenging air-flow energy to sustainably power temperature sensors, ACS Nano 9 (4) (2015) 4553–4562.

[26] X. Wang, Y. Yang, Effective energy storage from a hybridized electromagnetic-triboelectric nanogenerator, Nano Energy 32 (2017) 36–41.

[27] K. Zhang, X. Wang, Y. Yang, Z.L. Wang, Hybridized electromagnetictriboelectric nanogenerator for scavenging biomechanical energy for sustainably powering wearable electronics, ACS Nano 9 (4) (2015) 3521–3529.

[28] Z. Zhang, J. He, T. Wen, C. Zhai, J. Han, J. Mu, W. Jia, B. Zhang, W. Zhang, X. Chou, C. Xue, Magnetically levitated-triboelectric nanogenerator as a self-powered vibration monitoring sensor, Nano Energy 33 (2017) 88–97.

[29] H. Askari, E. Asadi, Z. Saadatnia, A. Khajepour, M.B. Khamesee, J. Zu, A hybridized electromagnetic-triboelectric self-powered sensor for traffic monitoring: concept, modelling, and optimization, Nano Energy 32 (2017) 105–116.

[30] M.-L. Seol, S.-B. Jeon, J.-W. Han, Y.-K. Choi, Ferrofluid-based triboelectric-elec-tromagnetic hybrid generator for sensitive and sustainable vibration energy harvesting, Nano Energy 31 (2017) 233–238.

[31] X. Ren, H. Fan, C. Wang, J. Ma, S. Lei, Y. Zhao, H. Li, N. Zhao, Magnetic force driven noncontact electromagnetic-triboelectric hybrid nanogenerator for scavenging biomechanical energy, Nano Energy 35 (2017) 233–241.

[32] K. Zhang, Z.L. Wang, Y. Yang, Conductive fabric-based stretchable hybridized na-nogenerator for scavenging biomechanical energy, ACS Nano 10 (4) (2016) 4728–4734.

[33] T. Quan, Z.L. Wang, Y. Yang, A shared-electrode-based hybridized electromagnetic-triboelectric nanogenerator, ACS Appl. Mater. Interfaces 8 (30) (2016) 19573–19578.

[34] L.-B. Huang, G. Bai, M.-C. Wong, Z. Yang, W. Xu, J. Hao, Magnetic-assisted non-contact triboelectric nanogenerator converting mechanical energy into electricity and light emissions, Adv. Mater. 28 (14) (2016) 2744–2751.

[35] L. biao Huang, W. Xu, G. Bai, M.-C. Wong, Z. Yang, J. Hao, Wind energy and blue energy harvesting based on magnetic-assisted noncontact triboelectric nanogen-erator, Nano Energy 30 (2016) 36–42.

[36] K. Zhang, Y. Yang, Linear-grating hybridized electromagnetic-triboelectric nano-generator for sustainably powering portable electronics, Nano Res. 9 (4) (2016) 974–984.

[37] R.K. Gupta, Q. Shi, L. Dhakar, T. Wang, C.H. Heng, C. Lee, Broadband energy harvester using non-linear polymer spring and electromagnetic/triboelectric hybrid mechanism, Sci. Rep. 7 (2017).

[38] X. Xia, G. Liu, L. Chen, W. Li, Y. Xi, H. Shi, C. Hu, Foldable and portable tribo-electric-electromagnetic generator for scavenging motion energy and as a sensitive gas flow sensor for detecting breath personality, Nanotechnology 26 (47) (2015) 475402.

[39] Y. Yang, Y.S. Zhou, H. Zhang, Y. Liu, S. Lee, Z.L. Wang, A single-electrode based triboelectric nanogenerator as self-powered tracking system, Adv. Mater. 25 (45) (2013) 6594–6601.

[40] E. Asadi, H. Askari, M.B. Khamesee, A. Khajepour, High frequency nano electro-magnetic self-powered sensor: concept, modelling and analysis, Measurement 107 (2017) 31–40.

[41] G. Xiao-fan, Y. Yong, Z. Xiao-jing, Analytic expression of magnetic field distribution of rectangular permanent magnets, Appl. Math. Mech. 25 (3) (2004) 297–306.

[42] X. Chen, S. Xu, N. Yao, Y. Shi, 1.6 v nanogenerator for mechanical energy har-vesting using pzt nanofibers, Nano Lett. 10 (6) (2010) 2133–2137.

[43] A. Ahmed, S.L. Zhang, I. Hassan, Z. Saadatnia, Y. Zi, J. Zu, Z.L. Wang, A washable, stretchable, and self-powered human-machine interfacing triboelectric nanogen-erator for wireless communications and soft robotics pressure sensor arrays, Extrem. Mech. Lett. 13 (2017) 25–35 (Supplement C).

[44] R. Cao, T. Zhou, B. Wang, Y. Yin, Z. Yuan, C. Li, Z.L. Wang, Rotating-sleeve tri-boelectric-electromagnetic hybrid nanogenerator for high efficiency of harvesting mechanical energy, ACS Nano 11 (8) (2017) 8370–8378.